

Article

Hydrothermally Synthesized Ag@MoS₂ Composite for Enhanced Photocatalytic Hydrogen Production

Anuja A. Yadav ^{1,†}, Yuvaraj M. Hunge ^{2,*}, Ananta G. Dhodamani ³ and Seok-Won Kang ¹

¹ Department of Automotive Engineering, Yeungnam University, 280 Daehak-ro, Gyeongsan 38541, Republic of Korea

² Research Institute of Science and Technology (RIST), Tokyo University of Science, 2641 Yamazaki, Noda 278-8510, Chiba, Japan

³ Department of Chemistry, Sadguru Gadage Maharaj College, Karad 415124, Maharashtra, India

* Correspondence: yuvarajhunge@gmail.com

† These authors contributed equally to this work.

Abstract: Photocatalytic hydrogen production is a green, cost-effective, simple, and pollution-free technology for the supply of clean energy, which plays an important role in alleviating the fossil fuel crisis caused by exponentially grown energy consumption. Therefore, designing highly visible-light-active novel photocatalyst materials for photocatalytic hydrogen production is a promising task. The production efficiency of photocatalyst can be improved by using noble metals, which are useful for the effective transfer of charge carriers. This study highlights the synergistic effect of the noble co-catalyst Ag on MoS₂ during the investigation of photocatalytic hydrogen production. The hydrothermal method was used for the preparation of an Ag-MoS₂ composite, and their structural and morphological characterizations were carried out using different physiochemical characterization techniques. The Ag-MoS₂ composite shows an enhanced visible light absorption capacity and photocatalytic hydrogen production rate, as compared to that of pure MoS₂, which proves that Ag nanoparticles (NPs) can act as efficient co-catalyst materials for photocatalytic hydrogen production with an improved rate of hydrogen production. Along with this, a possible working mechanism was proposed for visible-light-driven photocatalytic hydrogen production using the Ag@MoS₂ composite.

Keywords: Ag-MoS₂ composite; photocatalysis; hydrogen production; hydrothermal method



Citation: Yadav, A.A.; Hunge, Y.M.; Dhodamani, A.G.; Kang, S.-W. Hydrothermally Synthesized Ag@MoS₂ Composite for Enhanced Photocatalytic Hydrogen Production. *Catalysts* **2023**, *13*, 716. <https://doi.org/10.3390/catal13040716>

Academic Editors: Amr Fouda and Mohammed F. Hamza

Received: 8 March 2023

Revised: 24 March 2023

Accepted: 30 March 2023

Published: 10 April 2023



Copyright: © 2023 by the authors. Licensee MDPI, Basel, Switzerland. This article is an open access article distributed under the terms and conditions of the Creative Commons Attribution (CC BY) license (<https://creativecommons.org/licenses/by/4.0/>).

1. Introduction

Nowadays, the rapid growth of industrialization and increased populations have led to an enhanced demand for energy. To fulfill this energy demand, more pressure will be placed on natural resources, such as fossil fuels. Thus, the burning of fossil fuels leads to increased environmental pollution, which causes major problems of increased scarcity of fossil fuels, therefore worsening the energy crises in the upcoming future. Thus, it is important to develop different energy sources, such as wind, solar, geothermal, biomass, etc., which are clean, renewable, pollution-free, and sustainable energy sources [1–3]. However, the energy sources mentioned above have some major drawbacks and limitations, such as difficulties in their storage and transport and require high costs, and some sources (wind and solar) are regional, depending on location, etc. Among the different renewable energy sources, hydrogen energy is considered one of the best energy sources, owing to its good efficiency, being clean and pollution free and easy to handle, and its transport and storage are convenient. Several different techniques have been adopted to produce hydrogen gas, which include the steam reforming of hydrocarbons, the electrolysis of water, fermentation, the gasification of biomass, photocatalytic hydrogen production, etc. As compared to the photocatalytic hydrogen production method, the steam reforming of hydrocarbons method is an endothermic, reversible, and high-temperature reaction that generates CO₂, which further leads to the greenhouse effect [4]. Hence, photocatalytic hydrogen production

is a green technology in which photo-generated hydrogen can easily be stored, and it is a potential approach to meet energy demands. Hydrogen energy can be substituted for fossil fuels in the near future. The photocatalytic hydrogen production process is more economical, energy-saving, and produces clean hydrogen [4–7]. In this process, no electrical energy is required to initiate the process. Photocatalytic hydrogen production, using semiconductor-based photocatalyst materials, is of growing research interest among the research community to overcome the global energy crises [1,2]. Many efforts have been made in the development of highly efficient semiconductor photocatalyst materials and their use in photocatalytic hydrogen production through water-splitting reactions, but the efficiency of this process remains unsatisfactory due to the narrow solar spectral response, the high recombination of charge carriers, etc. [3]. Honda and Fujishima, in the 1970s, reported photocatalytic hydrogen evolution using a TiO₂ electrode for the first time [6]. Later, many semiconductor materials have been used to explore photocatalytic hydrogen production activity using metal oxides, sulfides, nitrides, etc. over the past few decades [8]. In the previous few decades, semiconductor materials, such as TiO₂ and ZnO, etc., due to their unique properties, such as their low cost, high thermal stability, high catalytic activity, chemical stability, etc., have been widely studied and used for various applications, such as solar cells, water splitting, hydrogen production, photocatalysis, air purification, etc. In addition, ZnO and TiO₂ possess direct bandgap energies of 3.37 and 3.30 eV, respectively, which restricts their photocatalytic activity under visible light illumination. Along with this, the recombination of photogenerated charge carriers is so high in both ZnO and TiO₂ because of its high exciton binding energy. In addition, it is responsible for photo-corrosion. Thus, it is important to develop visible-light-active photocatalyst materials [9–11].

Recently, transition metal dichalcogenides (TMDs) have been widely used in different applications, such as supercapacitors, water splitting, photocatalysis, etc., due to their sufficient properties, such as their photoelectrochemical stability, good charge carrier mobility, fast nonlinear response, etc. [10]. Molybdenum sulfide (MoS₂) is a two-dimensional material and exhibits a good response under visible light (450–700 nm) illumination. These properties of MoS₂ help to improve its charge transfer properties and light absorption capacity and the performance of the heterojunction. As with graphene, MoS₂ has a stratified structure of S-Mo-S atoms [9,12]. The lattice structure and morphology of MoS₂ play an important role in its catalytic performance. However, a major drawback of MoS₂ is the recombination of the photogenerated charge carriers in MoS₂ being higher, which directly impacts its photocatalytic efficiency. According to the literature study, the noble metal nanoparticles had great advantages, such as the avoidance of charge recombination, as well as enhanced light absorption capacity [13,14]. The plasmonic NPs of noble metal (Ag, Au, and Pt) play an important role in photocatalytic hydrogen production as co-catalysts [15]. The addition or decoration of these noble metals onto semiconductor photocatalyst materials, such as MoS₂, g-C₃N₄, TiO₂, ZnO, etc., will result in the development of the space charge region. The space charge region is helpful for effective charge separation and ultimately improves the photocatalytic efficiency of the process [9]. Surface plasmon resonance (SPR) will be generated using noble metals under visible light illumination, and it forms a strong and non-homogeneous electric field near to the semiconductor surface. Through this process, plasmonic energy is created, which will be used to avoid the recombination of photo-excited electrons. Simultaneously, it creates a plasmonic heating zone that will be used in chemical transformation for breaking water molecules [10,16].

Zhao et al. synthesized a Ag-MoS₂ nanohybrid composite using a laser-assisted technique and used it for gas sensing applications [17]. Liu et. al. prepared Ag-doped 1T-2H-MoS₂ as a photocatalyst and studied the degradation of Cr (VI) and MB and observed that Ag nanoparticles could significantly enhance the charges' separation efficiency [18]. Krishnan et al. prepared the Ag-MoS₂ composite using a combination of hydrothermal and wet-chemical methods for electrochemical nitrobenzene sensing [19]. Cheah et al. reported the facile synthesis of Ag/MoS₂ nanocomposite photocatalyst for visible-light driven photocatalytic hydrogen gas production and found that Ag NPs can act as an efficient

co-catalyst for the MoS₂ nanoflakes and later improve the hydrogen gas evolution rate. Additionally, they observed that, at 20 wt%, Ag-loading exhibits the highest photocatalytic activity with a hydrogen gas evolution of 179.5 $\mu\text{mol H}_2 \text{ gcat}^{-1}$ [7]. Sun et al. prepared Ag-MoS₂ as a photocatalyst and studied the chromium reduction (Cr (VI) reduced into Cr (III)) in an aqueous solution and observed that, in dark conditions, MoS₂ acts as an electron donor through its self-oxidation and Cr (VI) anions were electron acceptors [20]. Therefore, noble metals can enhance the light adsorption capacity and catalytic performance of composite or heterojunction.

In this study, Ag-MoS₂ composite photocatalyst was designed using the hydrothermal method. The prepared Ag-MoS₂ composite photocatalyst was analytically characterized using different characterization techniques, such as X-ray diffraction, Raman spectroscopy, X-ray photoelectron spectroscopy, scanning electron microscopy, UV-Vis spectroscopy, etc. The prepared Ag-MoS₂ composite photocatalyst and commercialized MoS₂ powder were used to study the photocatalytic hydrogen production activity. Photocatalytic hydrogen production activity shows that the Ag-MoS₂ composite photocatalyst exhibits a better photocatalytic performance than the commercialized MoS₂ powder. The effects of Ag on the light absorption capacity, photoluminescence, and photocatalytic properties of MoS₂ were investigated in detail, and the possible mechanisms that contribute to the improvement of visible-light driven photocatalytic performance for the Ag-MoS₂ composite are discussed. The current work exemplifies the potential of designing a composite photocatalyst material by integrating Ag NPs as co-catalyst onto MoS₂ for improved visible-light-driven photocatalytic hydrogen production, which can serve as one of the feasible approaches for the advancement of renewable energy research.

2. Results and Discussion

Structural characterizations of MoS₂ and Ag-MoS₂ composite photocatalysts were performed using X-ray diffraction, Raman spectroscopy, and X-ray photoelectron spectroscopy (XPS). Figure 1 displays the XRD patterns for MoS₂ and Ag@MoS₂ composite photocatalysts. XRD patterns were recorded by varying the diffraction angle (2θ) from 10 to 70°. For both MoS₂ and Ag@MoS₂, composite XRD patterns are polycrystalline. In the case of MoS₂, most prominent peaks were found at 2θ 14.40°, 32.80°, and 39.71°, which correspond to the (002), (100), and (103) planes, respectively. From the XRD pattern, the hexagonal crystal structure of MoS₂ is confirmed using PDF file no. 77-1716 [21]. While, in the case of the Ag/MoS₂ composite, some additional peaks were observed at 38.02°, as well as 64.36°, which were associated with the Ag. The peaks are well matched with the PDF file No. 04-0783, which confirms the face-centered cubic structure of Ag [22]. The symbol * denotes the Ag peaks. XRD results confirm the formation of the Ag-MoS₂ composite without any impurities. Further, the prepared Ag-MoS₂ composite is characterized using Raman spectroscopy and XPS spectroscopy.

The different types of bonding, vibrational modes, and defects were analyzed using Raman spectroscopy. Figure 2 displays the Raman spectra of MoS₂ and Ag-MoS₂ composite. For MoS₂, the major peak positioned at 379.43 cm^{-1} corresponds to E12g mode, which is associated with the in-plane opposite vibration of two S atoms [23]. The peaks were observed at 821.13 and 991.61 cm^{-1} due to the oxidation of MoS₂ by laser irradiation, leading to the formation of MoO₃, which presents the vibrational energy of MoO₃. Other major peaks found at 284.23 and 821.13 cm^{-1} are associated with MoS₂. In the case of the Ag-MoS₂ composite, the peaks found at 1066.33, 1301.89, and 1536.68 cm^{-1} are associated with Ag [24]. So, Raman investigation confirms the formation of a Ag-MoS₂ composite.

To understand the chemical composition and valence states of synthesized materials, X-ray photoelectron spectroscopy (XPS) study was conducted. Figure S1 presents the XPS spectrum of MoS₂. Figure S1a shows the high-resolution XPS spectrum of Mo 3d, which splits into Mo 3d 5/2 and Mo 3d 3/2 with binding energy at 229.12 and 232.3 eV. The S 2p spectrum (Figure S1b) shows two major peaks at binding energy 162.02 and 163.05 eV, while, in the case of oxygen (O 1s), peaks were found at binding energies of

529.89 and 532.32 eV (Figure S1c). The peaks at 529.89 and 532.32 eV correspond to lattice oxygen and OH^- groups, respectively [3]. Figure 3 presents the XPS study of the Ag-MoS₂ composite. Figure 3a presents the survey scan spectrum of the Ag-MoS₂ composite. It confirms the occurrence of Ag 3d, Mo 3d, S2p, and O 1s elements. No other impurity elements were detected. Figure 3b presents the Ag 3d spectrum, which splits into two major peaks having binding energy 373.56 and 367.51 eV, which confirm Ag 3d_{3/2} and Ag 3d_{5/2}, respectively [25]. Figure 3c displays the high-resolution Mo 3d spectrum. The Mo 3d spectrum splits into Mo 3d_{5/2} and Mo 3d_{3/2} with binding energies (BEs) of 229.02 and 232.21 eV, respectively [26]. The S2p spectrum is shown in Figure 3d. The S2p spectrum splits into two major peaks, having BE at 161.90 and 163.02 eV, which are associated with the S 2p_{3/2}, and S 2p_{1/2}, respectively [27]. The O 1s spectrum is shown in Figure 3e, and it is split into two major peaks with binding energies of 532.23 eV (O1) and 533.78 eV (O2), which correspond to the core level O₂, and S-O bonds, respectively [1,11]. Not much difference was observed in the binding energy of MoS₂, as compared to the MoS₂ presented in the Ag-MoS₂ composite [1].

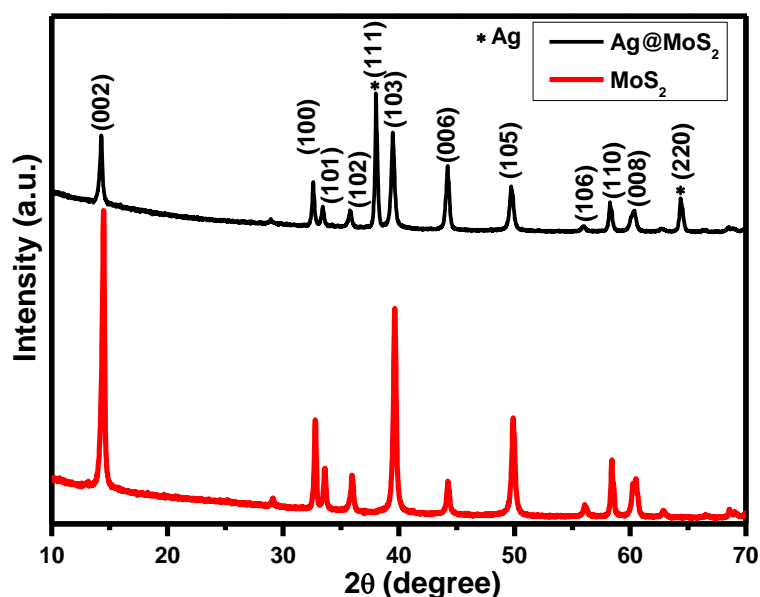


Figure 1. X-ray diffraction patterns of the MoS₂ and Ag-MoS₂ composites.

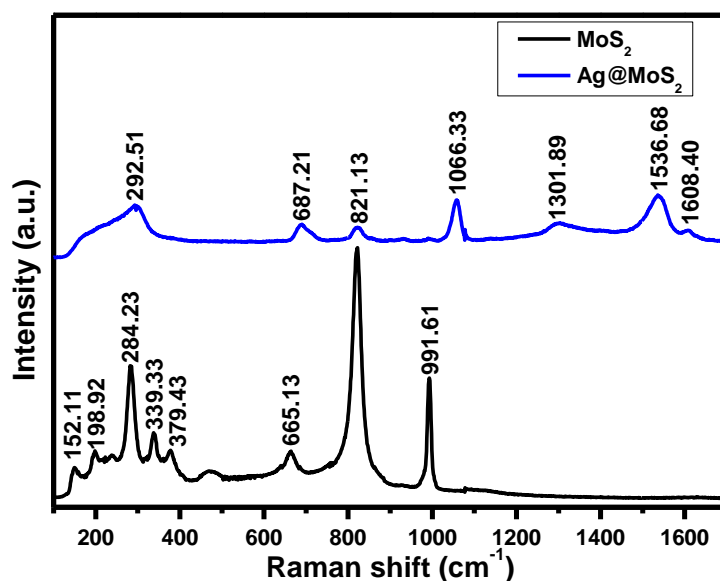


Figure 2. Raman spectra of MoS₂ and Ag-MoS₂ composites.

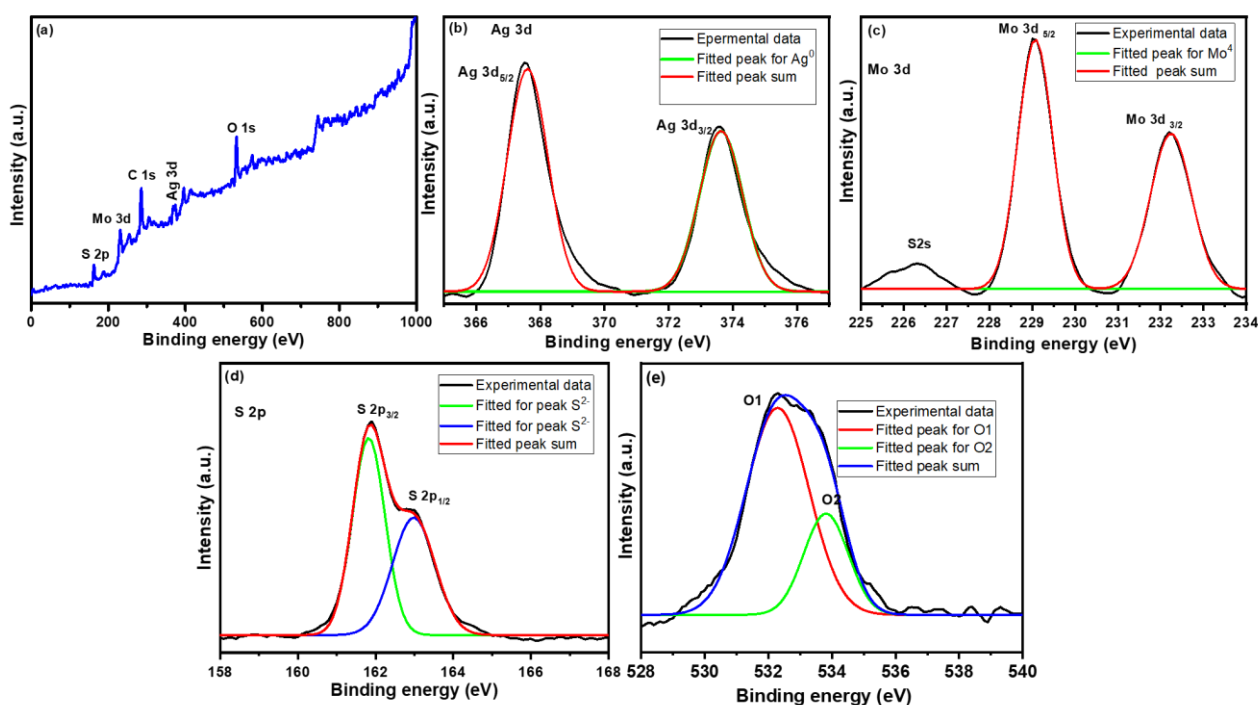


Figure 3. (a) X-ray photoelectron spectroscopy (XPS) spectrum of Ag/MoS₂ composite, (b) Ag 3d spectrum, (c) Mo 3sd spectrum, (d) S 2p spectrum, and (e) O 1s spectrum.

The morphological study provides information on the size and shape (i.e., the overall surface characteristics of the synthesized nanomaterials). Figure 4 shows scanning electron microscopy images of MoS₂ and Ag-MoS₂ composites at different magnifications. Figure 4a presents the scanning electron microscopy (SEM) image of MoS₂. For MoS₂, irregularly shaped and sized particles were found, and, in some places, particles agglomerated. While, in the case of the Ag-MoS₂ composite along MoS₂ particles, some hexagonal-shaped Ag particles are observed and presented in Figure 4b,c. Suber [28] observed similar morphology of hexagonal tabular-shaped silver particles.

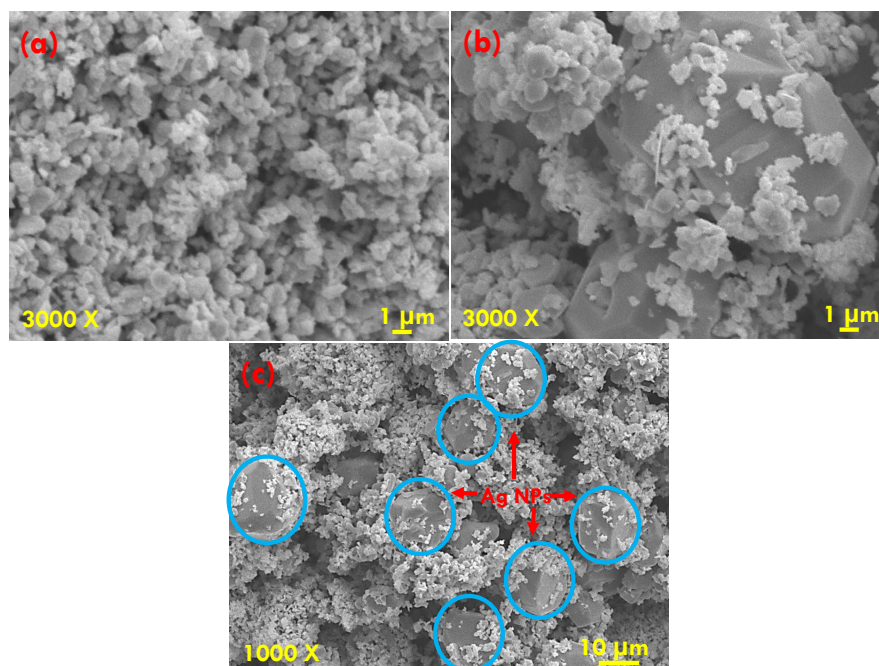


Figure 4. SEM micrographs of (a) MoS₂ and (b,c) Ag-MoS₂ composites at different magnification.

Optical properties are another significant parameter while investigating the photocatalytic properties of semiconductor materials. Figure 5a presents the absorbance spectra for MoS₂ and Ag-MoS₂ composites, scanned in the wavelength range of 350–1400 nm. MoS₂ has an absorption edge of nearly 900 nm, while, in the case of the Ag-MoS₂ composite, the absorption edge shifted towards a higher wavelength size (i.e., 925 nm). In the case of MoS₂, two separated exciton peaks are observed at 695 and 660 nm. No significant difference is observed in the absorption spectra of MoS₂ and the Ag-MoS₂ composite except for a minor difference in terms of absorption intensity. For the Ag-MoS₂ composite, enhanced visible light absorption was detected, which suggests the exclusive co-catalyst function of Ag. The following equation was used to calculate the band gap energy [29]:

$$\alpha h\nu = A(h\nu - E_g)^n$$

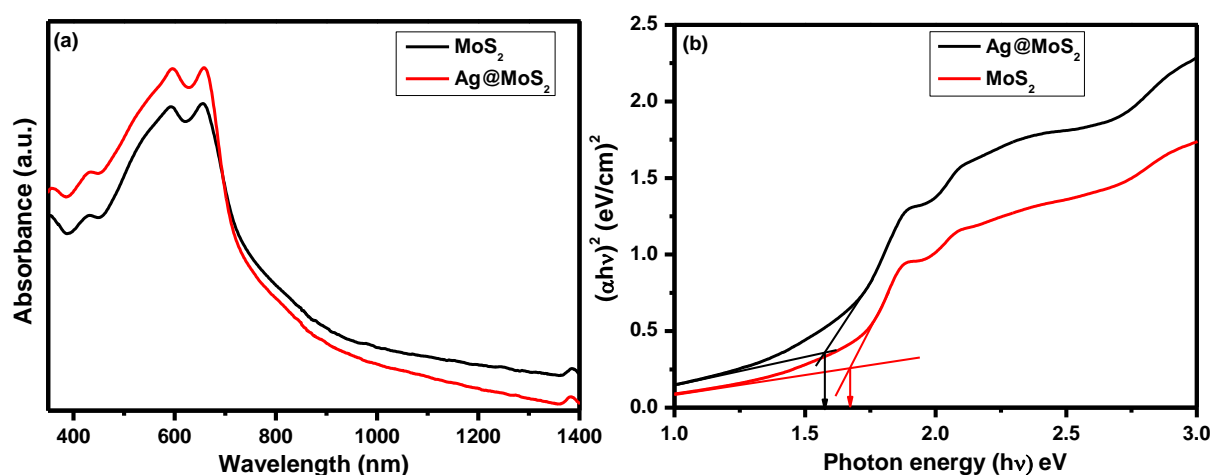


Figure 5. (a) Absorbance spectra and (b) band gap plots for the MoS₂ and Ag-MoS₂ composites.

The band gap energy values were found to be 1.57 and 1.67 eV for Ag-MoS₂ composites and MoS₂, respectively, and they are presented in Figure 5b. “A” is constant, n is order, E_g is band gap energy, and hν is the photon energy. The reduced bandgap energy of MoS₂, after its composite formation with Ag, suggests that there exists a change in the electronic structure of MoS₂ [30].

Photoluminescence (PL) spectroscopy was used to determine the recombination of photo-generated charge carriers in the catalyst. Recombination of photo-generated charge carriers is determined using fluorescence intensity. The higher the fluorescence intensity, the more there is recombination of charge carriers, and vice versa [1]. These photogenerated charge carriers facilitate redox reactions. Figure S2 shows the photoluminescence (PL) spectra of the MoS₂ and Ag-MoS₂ composite photocatalysts. The PL spectra for both of the samples showed a principal emission peak centered at around 660 nm. The lower PL emission intensity of the Ag-MoS₂ composite suggested that Ag nanoparticles hindered the recombination of the charge carrier (i.e., the highest charge separation efficiency) [11].

3. Photocatalytic Hydrogen Production Activity

Visible-light-driven photocatalytic hydrogen production activity of MoS₂ and Ag-MoS₂ composites were investigated and presented in Figure 6. Figure 6a presents the plot of hydrogen evolution as a function of illumination time. A hydrogen production experiment was conducted for 150 min. From the graph, it is revealed that the hydrogen evolution rate increased with increasing illumination time. For MoS₂ and Ag-MoS₂, the composite hydrogen gas production rates were found to be 24.8 and 43.4 μmol/h, respectively. Thus, the Ag-MoS₂ composite exhibits a better hydrogen production rate than MoS₂. The enhanced hydrogen production rate of the Ag-MoS₂ composite is attributed to “effective charge generation, separation, and transfer, along with more active sites available for redox reactions and minimum charge recombination” [3]. In addition, this

improvement is observed mainly due to the electron sink effect [31,32]. In the case of the Ag-MoS₂ composite, Ag particles act as a sink of electrons for those photoexcited electrons from MoS₂ and stop the recombination of charge carriers. Thus, photo-generated charge carriers trigger photocatalytic hydrogen evolution reactions [33]. To confirm the role of Ag nanoparticles for clarification, using the same experimental conditions, the photocatalytic activity of Ag NPs was also tested, and it was found that no trace amount of H₂ gas was detected after 150 min of reaction. From the above observation, it is confirmed that Ag nanoparticles were able to trigger the photosensitization process, which can be excluded, and the hydrogen gas evolution improvement is indeed contributed by the Ag NP that serve as a co-catalyst. The Ag-MoS₂ composite was selected for further study to observe the stability of the photocatalyst. The Table S1 comparison of photocatalytic hydrogen activity was proposed, using different photocatalysts.

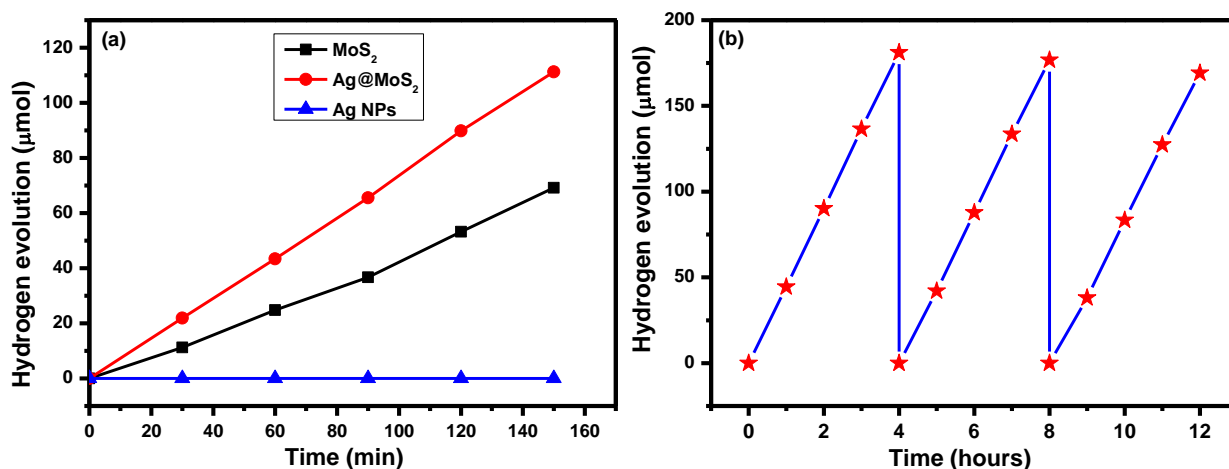


Figure 6. Photocatalytic H₂ production activity using MoS₂ and Ag-MoS₂ composites and Ag NPs: (a) cycling tests for photocatalytic H₂ production; (b) H₂ evolution in three consecutive 4 h cycles using Ag-MoS₂ composite. (★ indicate the amount of hydrogen produced.)

A photostability study of the Ag-MoS₂ composite was performed by recycling tests. The photostability study or recycling study is presented in Figure 6b. The stability study was conducted for up to three cycles and each cycle of four hours. From the plot, it is observed that the Ag-MoS₂ composite exhibits good stability. During the first cycle of four hours, 181.2 μmol hydrogen gas evolved. Up to the third cycle, 169.2 μmol hydrogen gas evolution was observed. There is a slight decrease in hydrogen production activity, which was detected after the third cycle. Photo-corrosion of photocatalysts and the loss of the photocatalyst during the recovery process are responsible for the decrease in H₂ production activity [34].

The photostability of the Ag-MoS₂ composite catalyst is determined by characterization techniques, such as X-ray diffraction study before and after the photocatalytic reaction was presented in Figure S3. Similar photocatalytic experimental conditions were used to check the stability. This photostability was checked three times using the Ag-MoS₂ composite photocatalyst. It showed that the recyclability of the Ag-MoS₂ composite photocatalyst was good. From the results, it was observed that the structure of the catalyst after the third cycle did not change much compared to before the photocatalytic experiment, except for the slight change in the XRD peak intensity.

The electron sink effect is responsible for the improvement in hydrogen production [31]. In the case of the Ag-MoS₂ composite, Ag nanoparticles act as a pool to gather photoexcited electrons from the MoS₂ and to stop the recombination of photogenerated charge carriers. These photoexcited electrons will be responsible for initiating the photocatalytic reactions and, thereby, enhancing the hydrogen gas production rate. From the UV-Vis absorption spectroscopy, it is observed that the absorption of the Ag-MoS₂ composites does not

change much, but the hydrogen gas evolution rate appears to be quite different. Making a composite of Ag with MoS₂ boosted the H₂ gas production rate [33].

Photocatalytic Mechanism Discussion

Ag nanoparticles served as co-catalysts in the Ag-MoS₂ composite, which is responsible for the improvement in the hydrogen gas evolution rate. Such a composite has encouraged the development of a space charge region and is presented in Figure S4. The space charge region will ease the effective charge separation. According to the literature, the Fermi energy level of MoS₂ lies in the potential range of 4.7–4.0 eV [35], and the Fermi energy level for Ag nanoparticles is 5.5 eV [36]. Such differences in Fermi energy levels (0.8–1.5 eV) result in the bending of bands and the formation of a space charge region at the interface of the Ag-MoS₂ composite [35]. The space charge region is a charge-free region and is occupied with a continuum of opposite charges. In this case, MoS₂ and Ag co-catalyst sides are occupied by negative and positive charges, respectively [37]. The positive and negative charges are distributed in a parallel manner and are separated by a gap (space charge region) [38]. Due to the high energy barrier, the movement of charge carriers is prevented, which results from the internal electric field under thermal equilibrium conditions. Upon illumination, the thermal equilibrium condition is disturbed by the incident photons, which causes the electric field in the space charge region to strictly promote the photoexcited electrons to bypass the potential barrier. After that, these photoexcited electrons will underpass through the space charge region and gather on the surface of the co-catalyst (Ag). Holes are left on the MoS₂ side. Hence, the formation of a space charge region can prevent the recombination of charge carriers and the effective separation of electrons–holes [39]. In the Ag-MoS₂ composite, Ag nanoparticles act as an electron pool for photoexcited electrons for the conversion of hydrogen ions to H₂ molecules. As compared to pure MoS₂, the reduction in water molecules is greatly eased at the surface of Ag nanoparticles, while oxidation reactions will take place on the active edges of the MoS₂. Na₂S and Na₂SO₃ were used as hole sacrificial agents to avoid the degradation of the composite. These sacrificial agents are widely used in sulfide-based photocatalyst materials [40]. It was found that the sulfur ions (S₂[−] and SO₃^{2−}) from these sacrificial agents (Na₂S and Na₂SO₃) provide an extra sulfur ion to enable surface reconstruction of the MoS₂, as well as prevent further oxidation of the MoS₂ [41]. Additionally, the sacrificial agents act as electron donors to react with the photo-generated holes [41,42], and they hence increase the tendency of the photo-generated electrons to transfer to the conduction band of the MoS₂.

The addition or incorporation of metal nanoparticles to semiconductor material acts as an alternative way to enhance the hydrogen gas evolution in water due to the fast transfer of the excited electrons generated by photon absorption from the semiconductor to the metal, which results in undesired recombination by deexcitation to the ground state severely inhibited. The contribution of the metal nanoparticles is more an important due to effective charge transfer within the composite if compared to the MoS₂. In the case of pure MoS₂, there is a high possibility for the recombination of excitons to occur [43].

4. Experimental Details

4.1. Chemicals

Molybdenum disulfide powder (MoS₂), sodium hydroxide (NaOH), silver nitrate (AgNO₃), sodium sulfite (Na₂SO₃), and sodium sulfide (Na₂S) were used. The above required chemicals were provided by Sigma Aldrich Company, Bengaluru, India.

4.2. Synthesis of the Ag@MoS₂ Composite

Commercialized MoS₂ was spread into a 20 mL mixture of deionized water (DI) and ethanol (2:8) for 30 min in the first flask. In another flask, 0.2 M of 9% weight percentage of AgNO₃ solution was prepared. Both solutions were mixed, and the suspension was stirred. Using a NaBH₄ aqueous solution, the reduction of Ag was achieved. The chemical reduction process was simple, cost-effective, environmentally friendly, and performed

at room temperature. An aqueous solution of NaBH_4 was added dropwise to the above solution. The reaction solution was moved to a sealed Teflon autoclave. The hydrothermal reactor was placed in a furnace for 12 h at 120 °C.

4.3. Characterizations

Crystal structures of the prepared materials were analyzed using X-ray diffraction (XRD; $\text{CuK}\alpha$ radiation ($\lambda = 1.5406 \text{ \AA}$) from a Bruker D2 Phaser, Mannheim, Germany). The Raman spectrum of the Ag-MoS₂ sample was analyzed using a Renishaw in Via Raman spectrometer using a He-Ne (633 nm) laser excitation source. Elemental composition was analyzed by X-ray photoelectron spectroscopy (XPS, Thermo Scientific, Waltham, MA, USA). The K-Alpha was set up by using a monochromatic Al K α X-ray source. The morphology of the prepared material was observed by using the SEM instrument JSM-7600F of the Japan Electron Optics Laboratory (JEOL, Tokyo, Japan). Optical properties were studied using UV-Vis absorption spectroscopy (Shimadzu: UV-1800, Kyoto, Japan). PL measurements were carried out on a micro-confocal Raman spectrometer (Horiba HR Evolution) equipped with an Olympus BX 41 microscope. The 532 nm laser was used as the excitation source.

4.4. Photocatalytic Hydrogen Production

The photocatalytic hydrogen production study was carried out in a closed Pyrex reactor using commercialized MoS₂ and Ag@MoS₂ composites. An amount of 300 W of the xenon arc lamp 172 mW/cm² with a UV cutoff filter ($\lambda > 420 \text{ nm}$) was used as a visible light source. For hydrogen production measurement, 25 mg amount of each catalyst was added into 50 mL of DI water containing 0.1 M Na₂S and 0.2 M Na₂SO₃. The formed solution was bubbled with N₂ gas for 30 min to remove the oxygen traces. After that, the reaction mixture was exposed to a light source. At different time intervals, gas samples were collected using a syringe. The photocatalytic reaction was performed under ambient conditions. An amount of 1 mL of gas was sampled every hour with a gas syringe and analyzed using gas chromatography (GC; GC-2014AT, Shimadzu, Japan; thermal conductivity detector, Ar carrier gas, molecular sieve 5 Å column) to quantify the gas composition.

5. Conclusions

Visible light-activated Ag-MoS₂ composite was successfully prepared using the hydrothermal method. The formation of the Ag-MoS₂ composite was confirmed using different techniques, such as X-ray diffraction, Raman spectroscopy, and X-ray photoelectron spectroscopy. X-ray diffraction study confirms the formation of Ag-MoS₂ composite with a hexagonal and face-centered cubic crystal structure of MoS₂ and Ag, respectively. Along with this, Raman spectroscopy and X-ray photoelectron spectroscopy confirm the formation of a Ag-MoS₂ composite. From the morphological investigation, it was observed that hexagonal-shaped Ag particles formed. An optical study proves that Ag-MoS₂ exhibits strong absorption in the visible region, with an energy bandgap of 1.57 eV. For MoS₂ and Ag-MoS₂ composites, hydrogen gas production rate was found to be 24.8 and 43.4 $\mu\text{mol/h}$, respectively. The Ag-MoS₂ composite exhibits nearly double the hydrogen production rate of the MoS₂, and this enhanced photocatalytic activity of the Ag-MoS₂ composite due to the electron sink effect. During the stability study, 181.2 and 169.2 μmol hydrogen gas evolved for the first and third cycles, respectively, which proves that Ag@MoS₂ exhibits good photostability.

Supplementary Materials: The following supporting information can be downloaded at: <https://www.mdpi.com/article/10.3390/catal13040716/s1>, Figure S1: XPS spectrum of MoS₂; Figure S2: Photoluminescence spectra of MoS₂ and Ag@MoS₂ composite; Figure S3: XRD patterns Ag@MoS₂ composite before and after (third cycle) the photocatalytic experiment; Figure S4: Schematic diagram of visible light hydrogen gas evolution over MoS₂ in the presence of Ag NPs as co-catalyst; Table S1: Comparison of photocatalytic hydrogen activity using different photocatalysts [7,44–46].

Author Contributions: Conceptualization, S.-W.K.; methodology, Y.M.H. and A.G.D. formal analysis, A.A.Y.; investigation, A.A.Y., Y.M.H. and A.A.Y.; writing—original draft preparation, Y.M.H. and A.A.Y.; writing—review and editing, A.A.Y., Y.M.H. and S.-W.K.; supervision, S.-W.K.; validation, S.-W.K.; project administration, S.-W.K.; funding acquisition, S.-W.K. All authors have read and agreed to the published version of the manuscript.

Funding: This research received no external funding.

Data Availability Statement: All data included in this study are available upon request by contact with the corresponding author.

Conflicts of Interest: The authors declare no conflict of interest.

References

1. Hunge, Y.M.; Yadav, A.A.; Kang, S.W.; Lim, S.J.; Kim, H. Visible Light Activated MoS₂/ZnO Composites for Photocatalytic Degradation of Ciprofloxacin Antibiotic and Hydrogen Production. *J. Photochem. Photobiol. A Chem.* **2023**, *434*, 11425. [\[CrossRef\]](#)
2. Vyas, Y.; Chundawat, P.; Dharmendra, D.; Punjabi, P.B.; Ameta, C. Review on Hydrogen Production Photocatalytically Using Carbon Quantum Dots: Future Fuel. *Int. J. Hydrogen Energy* **2021**, *46*, 37208–37241. [\[CrossRef\]](#)
3. Yadav, A.A.; Hunge, Y.M.; Kang, S.-W. Visible Light-Responsive CeO₂/MoS₂ Composite for Photocatalytic Hydrogen Production. *Catalysts* **2022**, *12*, 1185. [\[CrossRef\]](#)
4. Jiang, L.; Yang, J.; Zhou, S.; Yu, H.; Liang, J.; Chu, W.; Li, H.; Wang, H.; Wu, Z.; Yuan, X. Strategies to Extend Near-Infrared Light Harvest of Polymer Carbon Nitride Photocatalysts. *Coord. Chem. Rev.* **2021**, *439*, 213947. [\[CrossRef\]](#)
5. Swain, G.; Sultana, S.; Naik, B.; Parida, K. Coupling of Crumpled-Type Novel MoS₂ with CeO₂ Nanoparticles: A Noble-Metal-Free p–n Heterojunction Composite for Visible Light Photocatalytic H₂ Production. *ACS Omega* **2017**, *7*, 3745–3753. [\[CrossRef\]](#)
6. Fujishima, A.; Honda, K. Electrochemical Photolysis of Water at a Semiconductor Electrode. *Nature* **1972**, *238*, 37–38. [\[CrossRef\]](#)
7. Cheah, A.J.; Chiu, W.S.; Khiew, P.S.; Nakajima, H.; Saisopa, T.; Songsiriritthigul, P.; Radiman, S.; Hamid, M.A.A. Facile Synthesis of a Ag/MoS₂ Nanocomposite Photocatalyst for Enhanced Visible-Light Driven Hydrogen Gas Evolution. *Catal. Sci. Technol.* **2015**, *5*, 4133–4143. [\[CrossRef\]](#)
8. Yadav, A.; Hunge, Y.M.; Kang, S.W. Porous Nanoplate-Like Tungsten Trioxide/Reduced Graphene Oxide Catalyst for Sonocatalytic Degradation and Photocatalytic Hydrogen Production. *Surf. Interf.* **2021**, *24*, 101075. [\[CrossRef\]](#)
9. Hunge, Y.M.; Yadav, A.A.; Kang, S.W.; Kim, H. Photocatalytic Degradation of Tetracycline Antibiotics Using Hydrothermally Synthesized Two-Dimensional Molybdenum Disulfide/Titanium Dioxide Composites. *J. Colloid Inter. Sci.* **2021**, *606*, 454–463. [\[CrossRef\]](#)
10. Wei, R.; Tang, N.; Jiang, L.; Yang, J.; Guo, J.; Yuan, X.; Liang, J.; Zhu, Y.; Wu, Z.; Li, H. Bimetallic Nanoparticles Meet Polymeric Carbon Nitride: Fabrications, Catalytic Applications and Perspectives. *Coord. Chem. Rev.* **2022**, *462*, 214500. [\[CrossRef\]](#)
11. Hunge, Y.M.; Yadav, A.A.; Kang, S.W.; Kim, H. Facile Synthesis of Multitasking Composite of Silver Nanoparticle with Zinc Oxide for 4-Nitrophenol Reduction, Photocatalytic Hydrogen Production, and 4-Chlorophenol Degradation. *J. Alloy. Compd.* **2022**, *928*, 167133. [\[CrossRef\]](#)
12. Yang, J.; Wang, H.; Jiang, L.; Yu, H.; Zhao, Y.; Chen, H.; Yuan, X.; Liang, J.; Li, H.; Wu, Z. Defective Polymeric Carbon Nitride: Fabrications, Photocatalytic Applications and Perspectives. *Chem. Eng. J.* **2022**, *427*, 130991. [\[CrossRef\]](#)
13. Li, X.; Zhu, H. Two-Dimensional MoS₂: Properties, Preparation, and Applications. *J. Mater.* **2015**, *1*, 33–44. [\[CrossRef\]](#)
14. Samy, O.; Zeng, S.; Birowosuto, M.D.; El Moutaouakil, A. A Review on MoS₂ Properties, Synthesis, Sensing Applications and Challenges. *Crystals* **2021**, *11*, 355. [\[CrossRef\]](#)
15. Linic, S.; Christopher, P.; Ingram, D.B. Plasmonic-Metal Nanostructures for Efficient Conversion of Solar to Chemical Energy. *Nat. Mater.* **2011**, *10*, 911. [\[CrossRef\]](#)
16. Yang, X.; Yua, H.; Guo, X.; Ding, Q.; Pullerits, T.; Wang, R.; Zhang, G.; Liang, W.; Sun, M. Plasmon-Exciton Coupling of Monolayer MoS₂-Ag Nanoparticles Hybrids for Surface Catalytic Reaction. *Mater. Today Energy* **2017**, *5*, 72–78. [\[CrossRef\]](#)
17. Zhao, Y.; Deng, G.; Liu, X.; Sun, L.; Li, H.; Cheng, Q.; Xi, K.; Xu, D. MoS₂/Ag Nanohybrid: A Novel Matrix with Synergistic Effect for Small Molecule Drugs Analysis by Negative-Ion Matrix-Assisted Laser Desorption/Ionization Time-Of-Flight Mass Spectrometry. *Anal. Chim. Acta* **2016**, *937*, 87–95. [\[CrossRef\]](#)
18. Liu, H.; Wu, R.; Tian, L.; Kong, Y.; Sun, Y. Synergetic Photocatalytic Effect Between 1T@2H-MoS₂ and Plasmon Resonance Induced by Ag Quantum Dots. *Nanotechnology* **2018**, *29*, 285402–285413. [\[CrossRef\]](#)
19. Krishnan, U.; Kaur, M.; Singh, K.; Kaur, G.; Singh, P.; Kumar, M.; Kumar, A. MoS₂/Ag Nanocomposites for Electrochemical Sensing and Photocatalytic Degradation of Textile Pollutant. *J. Mater. Sci. Mater. Electron.* **2019**, *30*, 3711–3721. [\[CrossRef\]](#)
20. Sun, K.; Jia, F.; Yang, B.; Lin, C.; Li, X.; Song, S. Synergistic Effect in the Reduction of Cr(VI) with Ag-MoS₂ as Photocatalyst. *Appl. Mater. Today* **2020**, *18*, 100453. [\[CrossRef\]](#)
21. Gao, B.; Zhang, X. Synthesis of MoS₂ Inorganic Fullerene-Like Nanoparticles by a Chemical Vapour Deposition Method. *J. Chem.* **2014**, *67*, 6–11.
22. Georgekutty, R.; Seery, M.K.; Pillai, S.C. A Highly Efficient Ag-ZnO Photocatalyst: Synthesis, Properties, and Mechanism. *J. Phys. Chem. C* **2008**, *112*, 13563–13570. [\[CrossRef\]](#)

23. Cao, H.; Bai, Z.; Li, Y.; Xiao, Z.; Zhang, X.; Li, G. Solvothermal Synthesis of Defect-Rich Mixed 1T-2H MoS₂ Nanoflowers for Enhanced Hydrodesulfurization. *ACS Sustain. Chem. Eng.* **2020**, *819*, 7343–7352. [[CrossRef](#)]
24. Lai, C.H.; Wang, G.A.; Ling, T.K.; Wang, T.J.; Chiu, P.; Chau, Y.F.C.; Huang, C.C.; Chiang, H.P. Near Infrared Surface-Enhanced Raman Scattering Based on Star Shaped Gold/Silver Nanoparticles and Hyperbolic Metamaterial. *Sci. Rep.* **2017**, *7*, 5446. [[CrossRef](#)] [[PubMed](#)]
25. Alammari, T.; Mudring, A.V. Facile Preparation of Ag/ZnO Nanoparticles via Photoreduction. *J. Mater. Sci.* **2009**, *44*, 3218–3222. [[CrossRef](#)]
26. Fu, Y.; Ren, Z.; Wu, J.; Li, Y.; Liu, W.; Li, P.; Xing, L.; Ma, J.; Wang, H.; Xu, X. Direct Z-Scheme Heterojunction of ZnO/MoS₂ Nanoarrays Realized by Flowing-Induced Piezoelectric Field for Enhanced Sunlight Photocatalytic Performances. *Appl. Catal. B* **2021**, *285*, 119785. [[CrossRef](#)]
27. Jian, W.; Cheng, X.; Huang, Y.; You, Y.; Zhou, R.; Sun, T.; Xu, J. Arrays of ZnO/MoS₂ Nanocables and MoS₂ Nanotubes with Phase Engineering for Bifunctional Photoelectrochemical and Electrochemical Water Splitting. *Chem. Eng. J.* **2017**, *328*, 474–483. [[CrossRef](#)]
28. Suber, L. Formation and Oriented Aggregation of Tabular Hexagonal Silver Particles. *Condens. Matter* **2018**, *3*, 13. [[CrossRef](#)]
29. Yadav, A.A.; Kang, S.W.; Hunge, Y.M. Photocatalytic Degradation of Rhodamine B Using Graphitic Carbon Nitride Photocatalyst. *J. Mater. Sci. Mater. Electron.* **2021**, *3211*, 15577–15585. [[CrossRef](#)]
30. Yadav, A.A.; Hunge, Y.M.; Kang, S.W. Spongy Ball-Like Copper Oxide Nanostructure Modified by Reduced Graphene Oxide for Enhanced Photocatalytic Hydrogen Production. *Mater. Res. Bull.* **2021**, *133*, 111026. [[CrossRef](#)]
31. Sangpour, P.; Hashemi, F.; Moshfegh, A.Z. Photoenhanced Degradation of Methylene Blue on Cosputtered M:TiO₂ (M = Au, Ag, Cu) Nanocomposite Systems: A Comparative Study. *J. Phys. Chem. C* **2010**, *114*, 13955. [[CrossRef](#)]
32. Osterloh, F.E. Boosting the Efficiency of Suspended Photocatalysts for Overall Water Splitting. *J. Phys. Chem. Lett.* **2014**, *5*, 2510. [[CrossRef](#)]
33. Spinelli, P.; Polman, A. Prospects of Near-Field Plasmonic Absorption Enhancement in Semiconductor Materials Using Embedded Ag Nanoparticles. *Opt. Express* **2012**, *20*, A641–A654. [[CrossRef](#)]
34. Hunge, Y.M.; Yadav, A.A.; Mathe, V.L. Photocatalytic Hydrogen Production Using TiO₂ Nanogranules Prepared by Hydrothermal Route. *Chem. Phys. Lett.* **2019**, *731*, 136582. [[CrossRef](#)]
35. Bhanu, U.; Islam, M.R.; Tetard, L.; Khondaker, S. Photoluminescence Quenching in Gold-MoS₂ Hybrid Nanoflakes. *Sci. Rep.* **2014**, *4*, 5575. [[CrossRef](#)]
36. Baia, L.; Baia, M.; Kiefer, W.; Popp, J.; Simon, S. Prohibitin 2: At a Communications Crossroads. *Chem. Phys.* **2006**, *327*, 63. [[CrossRef](#)]
37. Poole, C., Jr. *Encyclopedic Dictionary of Condensed Matter Physics*; Academic Press: Cambridge, MA, USA, 2004.
38. Torimoto, T.; Horibe, H.; Kameyama, T.; Okazaki, K.-I.; Ikeda, S.; Matsumura, M.; Ishikawa, A.; Ishihara, H. Plasmon-Enhanced Photocatalytic Activity of Cadmium Sulfide Nanoparticle Immobilized on Silica-Coated Gold Particles. *J. Phys. Chem. Lett.* **2011**, *2*, 2057. [[CrossRef](#)]
39. Bumajdad, A.; Madkour, M. Understanding the Superior Photocatalytic Activity of Noble Metals Modified Titania Under UV and Visible Light Irradiation. *Phys. Chem. Chem. Phys.* **2014**, *1*, 7146. [[CrossRef](#)]
40. Zhang, J.; Yu, J.; Zhang, Y.; Li, Q.; Gong, J.R. Visible Light Photocatalytic H₂-Production Activity of CuS/ZnS Porous Nanosheets Based on Photoinduced Interfacial Charge Transfer. *Nano Lett.* **2011**, *11*, 4774. [[CrossRef](#)]
41. Schneider, J.; Bahnemann, D.W. Undesired Role of Sacrificial Reagents in Photocatalysis. *J. Phys. Chem. Lett.* **2013**, *4*, 3479. [[CrossRef](#)]
42. Li, N.; Liu, M.; Zhou, Z.; Zhou, J.; Sun, Y.; Guo, L. Charge Separation in Facet-Engineered Chalcogenide Photocatalyst: A Selective Photocorrosion Approach. *Nanoscale* **2014**, *6*, 9695. [[CrossRef](#)] [[PubMed](#)]
43. Wang, F.; Stepanov, P.; Gray, M.; Lau, C.N. Annealing and Transport Studies of Suspended Molybdenum Disulfide Devices. *Nanotechnology* **2015**, *26*, 105709. [[CrossRef](#)] [[PubMed](#)]
44. Lu, D.; Wang, H.; Zhao, X.; Kondamareddy, K.K.; Ding, J.; Li, C.; Fang, P. Highly efficient visible-light-induced photoactivity of Z-scheme g-C₃N₄/Ag/MoS₂ ternary photocatalysts for organic pollutant degradation and production of hydrogen. *ACS Sustain. Chem. Eng.* **2015**, *5*, 1436–1445. [[CrossRef](#)]
45. Shi, X.; Zhang, M.; Wang, X.; Kistanov, A.A.; Li, T.; Cao, W.; Huttula, M. Nickel nanoparticle-activated MoS₂ for efficient visible light photocatalytic hydrogen evolution. *Nanoscale* **2022**, *14*, 8601–8610. [[CrossRef](#)]
46. Gu, Q.; Sun, H.; Xie, Z.; Gao, Z.; Xue, C. MoS₂-coated microspheres of self-sensitized carbon nitride for efficient photocatalytic hydrogen generation under visible light irradiation. *Appl. Surf. Sci.* **2017**, *396*, 1808–1815. [[CrossRef](#)]

Disclaimer/Publisher's Note: The statements, opinions and data contained in all publications are solely those of the individual author(s) and contributor(s) and not of MDPI and/or the editor(s). MDPI and/or the editor(s) disclaim responsibility for any injury to people or property resulting from any ideas, methods, instructions or products referred to in the content.